Nanoscale

Accepted Manuscript

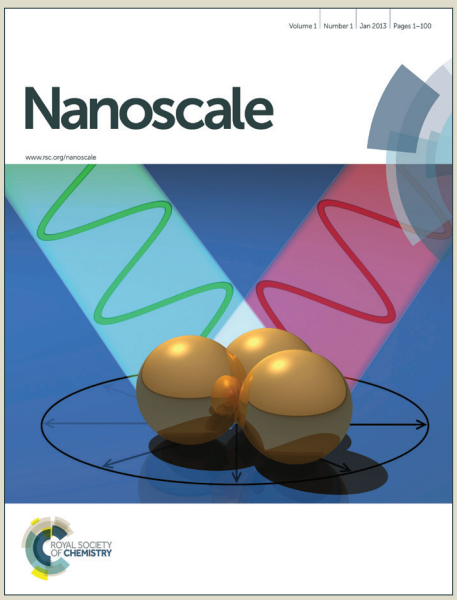

ROYAL SOCIETY OF CHEMISTRY

www.rsc.org/nanoscale

Revision Manuscript for *Nanoscale*

Ref. No.: NR-ART-01-2014-000288.R1

Formation and photovoltaic performance of few-layered graphene decorated TiO_2 nanocrystals used in dye-sensitized solar cells

Yueli Liu[a], Yuqing Cheng[a], Wei Shu[a], Zhuoyin Peng[a], Keqiang Chen[a], Jing Zhou[a], Wen Chen[a,*], Galina S. Zakharova[b]

[a] State Key Laboratory of Advanced Technology for Materials Synthesis and Processing, and School of Materials Science and Engineering, Wuhan University of Technology, Wuhan 430070, P. R. China

[b] Institute of Solid State Chemistry of the Ural Branch, Russian Academy of Science, Pervomaiskaya 91, Yekaterinburg 620219, Russia

Correspondent:

[*] Prof. W. Chen

Tel.: +86-27-8765-1107

Fax: +86-27-8776-0129

E-mail: **chenw@whut.edu.cn (Wen Chen)**

ABSTRACT

Few-layer graphene/TiO_2 nanocrystal composites are successfully in-situ synthesized in a low temperature of 400 °C using $C_{28}H_{16}Br_2$ as precursor. Raman mapping images show that the TiO_2 nanocrystals are very uniformly dispersed in the composite films and the in-situ coating during the thermal decomposition process will favor for the forming of the good interface combination between the few-layered graphene and TiO_2 nanocrystals. The few-layer graphene/TiO_2 nanocrystal composites are used as the photoanodes in the dye-sensitized solar cells (DSSCs), and the conversion efficiency of 8.25% is obtained under the full sun irradiation (AM 1.5), which increases by 65% comparing with that of the pure TiO_2 nanocrystal DSSCs (5.01%). It is found that the good interface combination between few-layered graphene and TiO_2 nanocrystals may improve the electric conductivity and life-time of photo-induced electrons in DSSCs. Moreover, some carbon atoms are doped into the crystal structure of the TiO_2 nanocrystals during the thermal decomposition process, which will enhance the light absorption by narrowing their band gap and favor for the improvement of the photovoltaic efficiency.

Keywords: Low-temperature synthesis, few-layer graphene/TiO_2 nanocrystal composites, dye-sensitized solar cells, interface combination, Raman mapping image

1. Introduction

Dye-sensitized solar cells (DSSCs) have been considered one of the most potential power sources because of their relative low cost and high conversion efficiency of 13 % [1-2]. In the past twenty years, many efforts have been paid to promote their conversion efficiency by designing and modifying the TiO_2 (P25)-based photoanode film, as it is the most important section of the DSSCs [3-4]. However, the common TiO_2 particles have limited application in the DSSCs due to their low electronic conductivity [5].

Strategies using graphene/TiO_2 nanocrystal composites have been proposed to solve the above problems [6], as graphene has many special physical properties, such as superior charge carries mobility at room temperature (more than 200000 $cm^2V^{-1}s^{-1}$), high surface area of over 2600 m^2/g, and so on [7-10]. Thus, graphene sheets between TiO_2 nanoparticles may enhance electron transporting ability and reduce the recombination of photo-induced electrons and holes. Many kinds of methods have been proposed to prepare the graphene/TiO_2 hybrid composites in DSSCs. For example, Graphene was incorporated with nanostructured TiO_2 films via molecular grafting for dye-sensitized solar cell application [11]. Electro-spinning method was used for the fabrication of one-dimensional TiO_2/graphene composites, which were used in the DSSCs and photo-degradation of methyl orange [12]. Graphene/TiO_2 composites were synthesized under control by a one-step solvothermal approach for the high performance DSSCs [13]. Sun et al. utilized the heterogeneous coagulation between Nafion-coated graphene and commercial TiO_2 (P25) nanoparticles as

photoanodes in DSSCs, and the photovoltaic efficiency was of 59% higher than that of pure P25 nanoparticles [6].

Nevertheless, most of them are prepared in a complicated method or are mechanical mixtures of graphene and nanomaterials, and it is still a great challenge to prepare the well-combined graphene and TiO_2 nanomaterials [14-16]. As graphene existed between the TiO_2 nanoparticles act as the rapid electron transfer path for the photo-induced electrons, which may improve the electric conductivity and life-time of photo-induced electrons [17-18]. Recently, Cheng et al. developed a two-step approach to synthesize TiO_2/reduced graphene oxide composites, it was found that the in-situ hydrolysis of the reduced graphene oxide favored for the enhancement of the conversion efficiency of DSSCs [18]. Cai et al. reported that $C_{28}H_{16}Br_2$ (a high symmetrical structure and high carbon content) was used as the precursor to prepare graphene nanoribbons on the (111) surface of Au and Ag at a relative low temperature of 400 °C [19], which provides an effective route for the forming of the well-combined graphene hybrid composites, and this is also a good example to prepare graphene/TiO_2 nanocrystal composites in DSSCs.

In the present work, we extended this facile process to coat the TiO_2 particles with few-layer graphene (FLG) at a relatively low temperature of 400 °C by using $C_{28}H_{16}Br_2$ as precursor. Then the composite materials were used as photoanodes in DSSCs by screen–printing technique, and it is found that the composites have a great enhancement on the photocurrent and conversion efficiency.

2. Experimental

2.1 Materials

P25 with the diameter of 30 nm is purchased from Degussa Co., Ltd. in Germany, N719 dye ($[(C_4H_9)_4N]_2[Ru(II)L_2(NCS)_2]$) is bought from Solaronix Co., Ltd. in Switzerland, and FTO conducting glass from Nippon Sheet Glass Co., Ltd. in Japan with the sheet resistance of 8 Ωcm^{-2}. All of the other chemical reagents used in the experiments are of analytical grade, purchased from Sinopharm Chemical Reagent Co., Ltd., and used without further purification.

2.2 Synthesis of graphene/TiO_2 composite materials films

The TiO_2 (P25) nanocrystals were added to the $C_{28}H_{16}Br_2$ (at a different weight ratio of TiO_2: $C_{28}H_{16}Br_2$) tetrahydrofuran solution, and the mixture was stirred vigorously. After the evaporation of the tetrahydrofuran, the mixture of TiO_2 and $C_{28}H_{16}Br_2$ was heat-treated at 200 °C for 30 min and then calcined at 400 °C for several hours in an argon atmosphere. Then the rough surfaces of the TiO_2 nanoparticles were successfully coated with few-layer graphene (FLG) after evaporating the organic solvent to obtain the resultant materials, and it was designated as FLG/TiO_2.

FLG/TiO_2 composite pastes were synthesized according to the Grätzel method [20]. Before preparing the photoanode films, FTO conducting glass was immersed into a 40 mM aqueous $TiCl_4$ solution at 70 ºC for 30 min, and then the pastes were coated on it to prepare a 0.5 × 0.5 cm^2 sized film by screen–printing technique (250 T mesh/inch, polyester). Additionally, the scattering layer with nanoparticles (>200nm) was also coated on the surface of the above film by doctor-blade method. Then, the

films were gradually annealed under air flow at 325ºC for 5 min, at 375ºC for 5min, at 450ºC for 15min and 500ºC for 15 min in order with the temperature rate of 5ºC/min. For comparison, TiO_2 nanocrystal films were also prepared in the same condition.

2.3 Fabrication of the dye-sensitized solar cell

The solar cell was fabricated by assembling spinning Pt counter electrode and N719 dye sensitized FLG/TiO_2 composites films on FTO conducting glass. The solar cell was sealed by using a Surlyn thermoplastic frame. A standard redox electrolyte was prepared by dissolving 0.05 M I_2, 0.5 M LiI, 0.3 M DMPII and 0.5 M 4-TBP in acetonitrile solution.

2.4 Characterization

The crystal structures and morphologies of the samples were characterized by X-ray diffraction (XRD, PertPro, PANalytical, Netherlands), Transmission electron microscope (TEM, JEM-2100F, JEOL, Japan), respectively. 3D Raman mapping image was measured by Confocal Raman System (WITec alpha300R, Germany) equipped with a 532 nm laser and optical diffraction limit of ~ 200 nm, the composite films were detected to obtain 3D information from the area of 100 μm×100 μm with a mesh of 2 μm at the center of FLG/TiO_2 composite films. X-ray photoelectron spectroscopy (XPS) measurement was performed in the Escalabmk-Ⅱ XPS apparatus (VG Scientific, England) with Al target. The emission angle between the photoelectron beam and the sample surface was 45°, and the calibration of the binding energy of the electron spectrometer was made by using the maximum adventitious C1s signal at 284.6 eV with the solution of the full width at half maximum (FWHM)

being 0.8 eV. Electrochemical impedance spectroscopy (EIS) was used to investigate electronic and ionic processes in DSSCs by Autolab Potentiostat 30 system (Metrohm, Switzerland) at the output frequency of 10^6 Hz-0.01Hz at an applied bias of V_{oc} with AC amplitude of 10 mV. Full sun conversion efficiency was characterized by the Keithley 4200 semiconductor characterization system (Keithley Instruments, USA) (Newport 91160, 300 W xenon lamp, USA). The light intensity of the illumination under AM 1.5 condition was determined using a reference monocrystalline silicon cell system (Oriel, USA).

3. Results and discussion

XRD patterns of the samples in Fig. 1(a) show that the diffraction peaks are originated from the anatase and rutile TiO_2 phases, and also identify that the relative content of anatase phase and rutile phase is about 4:1, which matches well with that of P25. Meanwhile, after decorated with FLG, there is no obvious peak change at the various contents of the FLG/TiO_2 composites, which is related to the fact that the FLG content is too little to be detected by XRD observation. However, there is a broadened peak in the range of 20-30 degree for the various FLG/TiO_2 composites.

Fig. 1(b) shows the FTIR spectra of the TiO_2 nanocrystals and as-prepared FLG/TiO_2 (0.75 wt %). For TiO_2 nanocrystals, the absorption peaks at 3602 cm^{-1} and 1621 cm^{-1} come from the –OH stretching group, while the wide peaks at 400-900 cm^{-1} originate from the stretching vibration of Ti-O-Ti bonds in crystalline TiO_2 [21-22]. However, for the FLG/TiO_2 composites, the broad absorption below 1000 cm^{-1} is much plumper with a sharp peak than the corresponding peak in pure TiO_2

nanocrystals, which is attributed to be the presence of Ti-O-Ti vibration and Ti-O-C vibration (805 cm^{-1}) [23-24], and the existence of the Ti-O-C bonds shows that the chemically bonded FLG/TiO_2 composites are formed by the thermal decomposition of $C_{28}H_{16}Br_2$ [25]. Moreover, it is clear that the FTIR spectrum of the FLG/TiO_2 composite shows some strong absorption peaks that correspond to the different oxygen functional groups, such as CH_2 group (2925 cm^{-1}) and alcoholic C-OH stretching (1442 cm^{-1}). Besides them, the absorption band at 1543 cm^{-1} clearly shows the skeletal vibration of the graphene sheets, indicating the in-situ formation of the few-layer graphene by the thermal decomposition of $C_{28}H_{16}Br_2$ [24].

From the TEM image of the 0.75 wt% FLG/TiO_2 composite in Fig. 2, some pieces of amorphous carbon can be clearly observed between the TiO_2 nanocrystals, which may be used to explain the broadened peak during 20-30 degree in XRD patterns in Fig. 1(a). Furthermore, the HRTEM image reveals that there are straight lattice fringes with inter-planar spacing of 3.57 Å and 3.25 Å, which correspond to the (101) planes of anatase TiO_2 and (110) planes of rutile TiO_2 from the XRD patterns, respectively, and the insetted FFT HRTEM image processed by FFT method in Fig. 2(b) shows the existence of the TiO_2 phase. This result further confirms that the TiO_2 crystal structure is well maintained after graphene coating, which is accord with the FTIR result in Fig. 1(b). Interestingly, an ultra-thin graphene layer is observed between the TiO_2 crystal samples, and its thickness is less than 1 nm. By selecting only the matrix reflections of the rectangle area in Fig. 2(b), the typical feature of the hexagonal structure of few-layer graphene is observed by the FFT HRTEM image

processed by FFT in Fig. 2(c) [26], which is quite different with that of the TiO_2 crystal insetted in Fig. 2(b). Therefore, it clearly shows that the FLG is tightly combined with the few-layer graphene by this kind of the in-situ pyrolyzation process.

Raman spectroscopy is a powerful tool for detecting carbon molecules and investigating their crystallization degree. Fig. 3(a) shows that the FLG and TiO_2 nanocrystals are uniformly dispersed in the formed film. Fig. 3(b) shows the Raman spectrum obtained by the zone in Fig. 3(a), and the characteristic peaks at 148 cm^{-1} ($E_{g(1)}$), 391 cm^{-1} (B_{1g}), 516 cm^{-1} (A_{1g}) and 637 cm^{-1} ($E_{g(2)}$) reveal that the existence of TiO_2 [27]. The bands located at 1352 and 1614 cm^{-1} correspond to the D (breathing mode of A_{1g} symmetry) and G (E_{2g} symmetry, in-plane bond-stretching motion of pairs of sp^2 C atoms) bands, respectively, which are the typical bonds of the graphitic materials. The G band is a typical zone center vibration mode of graphite crystalline, corresponding to order sp^2 bonded carbon, whereas the D band is an edge vibration mode or disorder layer. The sharp peaks and narrow full width at half maximum of the G and D bands indicate a high graphitization degree of the carbon coating layer, which is impossible to be achieved from the other carbon precursors (e.g., sugar) paralyzed at such low temperatures [19]. The 2D peak at 2671 cm^{-1} is symmetric with a full width at half maximum of 39 cm^{-1}, which is well fitted by a Lorentzian fit as indicated by the red fitted curve shown in Fig. 3(a), and the magnified spectrum around the 2D peak is insetted in Fig. 3(b). On the basis of the Raman spectrum in Fig. 3(b) and HRTEM results in Fig. 2, we could conclude that the coating layer is few-layer graphene (FLG) [24, 28-29].

How to investigate the interface combination of the FLG/TiO_2 composite films is quite important to reveal the resultant quality and structural properties of the graphene based hybrid films. Raman mapping image from Raman spectroscopy arises as a fast and useful tool for the distribution characterization of the composites containing carbon nanostructures [24], as Raman spectra of TiO_2 and graphene show non-overlapping well-defined features, which provides the valuable distribution information of the two components that can help to build a complete description of FLG/TiO_2 composite films. The Raman data are reorganized into intensity mapping, and Fig. 3(c) and 3(d) show the Raman mapping image of FLG/TiO_2 composite films. Fig. 3(c) shows the image obtained from the 2D bands of the graphene. The 'bright' regions with high intensity show the existence of the graphene, while the 'dark' regions are related with the information of TiO_2 nanocrystals, which confirms the uniform distribution of the graphene in the composite film. The strongest band of anatase TiO_2 (E_g mode around 148 cm^{-1}) is selected as the TiO_2 fingerprint, and the Raman mapping in Fig. 3(d) also shows that the TiO_2 nanocrystals are quite uniformly dispersed in the composite films. Therefore, the few-layer graphene may be fairly homogeneously formed in the composite films by in-situ pyrolyzation process.

UV-Vis spectra are used to character the optical absorption of all of the above samples in the wavelength range of 300-800 nm (Fig. 4). It shows that the FLG/TiO_2 composite films possess an obvious enhanced UV and visible light absorption comparing with TiO_2 nanocrystals, and the 0.75 wt% FLG/TiO_2 composite has the highest optical absorption intensity. Moreover, the absorption edge of FLG/TiO_2

composites shows a slight red-shift (403 nm), which is due to the formation of the C-doped TiO_2 nanocrystals during the formation process of FLG/TiO_2 composite [30]. Illustrated in Figure 4(b), by C doping, the electron produced under the irradiation by sun light may be excited from the valence band to the conduction band (process A) or from the C impurity level to the conduction band (process B). Therefore, the improvement of the optical absorption ability of the FLG/TiO_2 composite is due to the band gap narrowing and the enhancement of the utilization efficiency of solar energy by C doping [32]. Moreover, the well-combined FLG with TiO_2 nanocrystals in the composites also favor for the rapid transferring of the photo-generated electrons and reduce the recombination of the photo-generated electrons and holes in the FLG/TiO_2 composite.

XPS results reveal that the 0.75 wt% FLG/TiO_2 composite contains three elements of Ti, O, and C in XPS survey spectrum in Fig. 5(a). To investigate the carbon chemical states in the sample, the C 1*s* core levels are illustrated in Fig. 5(b). For the FLG/TiO_2 composite, two peaks with the binding energies of 284.61 and 281.68 eV coexist. Generally, the peak at 284.54 eV is a signal of adventitious elemental carbon [31-32], which originates from the graphitic sp^2 carbon atoms [18]. As there is no existence of the formations of C-O specie on the surface of the composite film from the FTIR spectra in Fig. 1(b), which also confirms that the existence of the graphene instead of graphene oxide (GO) [18]. While the peak at 281.24 eV is associated with Ti-C bonds (cation C^{2-} doped), indicating that carbon atoms substitute for some oxygen atoms into the O-Ti-O lattice and form the O-Ti-C

bonds during the in-situ pyrolyzation process, and the C-doping in composites could induce to the red-shift of absorption edge to visible light region shown in Fig. 4. Ti 2*p* spectrum in Fig. 5(c) shows that 2*p*3/2 peak of Ti element locates at 464.17 eV, and 1s peak of O^{2-} valence state is located at 531.33 eV with the absorbed O substance observed at 529.59 eV in Fig. 5(d).

Fig. 6(a) shows the cross-section SEM image of 0.75 wt% FLG/TiO_2 composite film, which displays that the film thickness is about 15 μm. Performance optimization of the electrodes is illustrated by photocurrent density-voltage (J-V) curves under AM 1.5 condition shown in Fig. 6(b), and the detailed performances are listed in Table 1. Choosing the total active cell area of 0.25 cm^2, the solar cells with the pure TiO_2 nanocrystals without graphene possess the short-circuit current density (J_{sc}) of 13.55 $mAcm^{-2}$, open-circuit voltage (V_{oc}) of 651 mV, fill factor (FF) of 0.568 and energy conversion efficiency (η) of 5.01%. Interestingly, the photoelectric performances will be enhanced by using the FLG/TiO_2 composite materials, and when the graphene amount is 0.75 wt%, the corresponding performance is the best one with J_{sc} of 18.03 $mAcm^{-2}$, V_{oc} of 686 mV, FF of 0.667 and η of 8.25%, respectively. Therefore, the conversion efficiency and fill factor increase by 65% and 18% with applying graphene in the 0.75 wt% FLG/TiO_2 composites, respectively.

Normally, the value of V_{oc} is determined by the potential difference between the Fermi level of TiO_2 and the chemical potential of the redox species (E_{red}) in the electrolyte as described in Equation (1) [33], in which γ is the characteristic constant of TiO_2 tailing states, k_B is the Boltzmann constant, T is temperature, e is the

elementary charge, and N_e is the effective density of states at the TiO_2 conduction band edge.

$$V_{oc} = E_{red} - E_{CB} - \gamma \frac{\kappa_B T}{e} \ln(\frac{N_e}{n}) \qquad (1)$$

In general, the E_{red} and E_{CB} would not change severely in DSSCs fabricated under similar conditions. V_{oc} is determined by the potential of the electron density (n) in TiO_2, and it is influenced by the surface charge and charge recombination. The V_{oc} will increase with the increasing of electron density (n) in the conduction band (CB) of TiO_2. After decorated with few-layer graphene, some carbon atoms are doped into the crystal structure of the TiO_2 nanocrystals and form the carbon impurity level inside the band gap, as proven by the UV-Vis spectra in Fig. 4(a) and XPS spectra in Fig. 5. Moreover, the well-combined graphene and TiO_2 nanocrystals will also favor for the fast transferring of the photo-excited electrons from the TiO_2 CB to the external circuit as shown in Fig. 4(b), which will be proved by the electrochemical impedance spectrum (EIS) data. Therefore, the narrowed band gap and the fast transferring ability of the photo-excited electrons of the FLG/TiO_2 composites will increase electron density (n) in the conduction band (CB) of TiO_2 nanocrystals, and thus increase the V_{oc} with the formation of the FLG/TiO_2 composites, as shown in Table 1.

The incident photon-to-current conversion efficiency (IPCE) is defined by the adsorption of the dye molecules in Fig. 6(c). Firstly, the improvement of IPCE is due to the high adsorption of the dye molecules and the low charge recombination. Moreover, the IPCE curves in Fig. 6(c) are well fitted with the absorption spectra of

dye molecules, and it is believed that the most IPCE peaks originate from the dye molecules' absorption. Secondly, the optical absorption at about 530 nm is assigned to $^2B_{2g} \rightarrow {}^2B_{1g}$ transition of 3*d* electrons of the Ti^{3+} ions [34], and the excitation of Ti ions has some certain contribution to the IPCE plots in a certain extent. Therefore, the above two factors have a synergism effect on the IPCE curve. Interesting, the IPCE spectra of the FLG/TiO_2 electrodes show a great enhancement in the conversion efficiency in the light region of 350-700 nm comparing with the pure TiO_2 nanocrystal electrodes. Therefore, it is believed that the increasing of maximum IPCE value from 25% to 68% is due to the few layer graphene exiting between the TiO_2 nanocrystals.

EIS spectrum is a widely-used technique to characterize the interfacial electrical property of DSSCs at an applied bias with AC amplitude of 10 mV under the one full sun illumination. It is noticed that there are two main semicircles observed in Fig. 7(a). In order to match well with the above EIS data, the equivalent circuit of the DSSCs is also to explain the transportation and recombination processes of the exciting electrons in the cells as shown in Fig. 7(a). The fitted R_s represents that the series resistance accounting for the transport resistance of the FTO and the electrolyte. R_{ct} and C_μ are the charge recombination resistance and the chemical capacitance at the dye-sensitized TiO_2/electrolyte interface, respectively. While R_{pt} and C_{pt} are charges transfer resistance at electrolyte/Pt/FTO interface and the interfacial capacitance, respectively.

From the Nyquist plots in Fig. 7(a), R_s of various films with or without the composition of the FLG is almost the same, which means that the resistance of FTO

and the electrolyte has no change in spite of using different materials. However, the FLG/TiO_2 composites photoanodes have smaller values of 18.0 Ω for R_{ct} comparing with 23.1 Ω of pure TiO_2 nanocrystal photoanodes from Table 1, which clearly implies that the enhanced transfer of the charge carriers between the TiO_2 film and electrolyte with the decoration of the FLG due to the perfect mobility of charger carriers of the FLG. Moreover, electron life-time (τ) is another important parameter for DSSCs, it can be extracted from the C_μ and R_{ct} using $\tau = C_\mu R_{ct}$ by fitting the EIS curves. The FLG/TiO_2 composites have the longer life-time than that of the pure TiO_2 nanocrystals. More importantly, the 0.75 wt% FLG/TiO_2 composites have the longest life-time (53.1ms), which is consistent with the date of energy conversion efficiency in Fig. 6(a). Therefore, the improvement of photoelectric performances of DSSCs of FLG/TiO_2 composites in Fig. 6(a), such as the fill factor, lies in the presence of FLG between TiO_2 nanoparticles, which may improve the intrinsic conductivity and life-time of electrons of the photoanodes by decreasing the value of R_{ct} in Fig. 7(a) [35-36].

Moreover, Bode plots in Fig. 7(b) also proves that the frequency of the second semicircle peak for the 0.75 wt% FLG/TiO_2 composites shifts to lower frequency comparing with that of the pure TiO_2 nanocrystals films, which presents a longer life-time of the electrons in the photoanode, and this is accord with the EIS result in Fig. 7(a).

4. Conclusions

The few-layer grapehene/TiO_2 composites were synthesized in a low temperature

by thermolysis method, and used as the photoanodes films to improve the conversion efficiency in DSSCs. The DSSCs based on 0.75 wt% FLG/TiO_2 composites possess the highest conversion efficiency of 8.25%, which increases by 65% comparing with that of the pure TiO_2 nanocrystal photoanodes (5.01%). Raman mapping images and EIS curves prove that the well-combined interface between TiO_2 nanocrystals and graphene will induce the lower charger recombination and faster transfer of the photoexcited electrons between the TiO_2 films and electrolytes. UV-Vis spectra show that the light absorption of the FLG/TiO_2 composites will be enhanced with a red-shift, which is related with the fact that both of the C-doped TiO_2 and FLG/TiO_2 composites are formed during the in-situ thermal decomposition process.

Acknowledgements

This work is supported by the International S&T Cooperation program of China (ISTCP) ((No. 2013DFR50710) and the National Nature Science Foundation of China (No. 50802070).

References

[1] J. Burschka, N. Pellet, S. Moon, R Humphry-Baker, P. Gao, M. K. Nazeeruddin and M. Grätzel, *Nature*, 2013, 499, 316-319.

[2] M. Z. Liu, M. B. Johnston and H. J. Snaith, *Nature*, 2013, 501, 395-398.

[3] K. Park, Q. Zhang and B. B. Garcia, *J. Phys. Chem. C*, 2011, 115, 4927-4934.

[4] Y. Li, W. Lee and D. K. Lee, *Appl. Phys. Lett.*, 2011, 98, 103301.

[5] B. O'Regan and M. Gratzel, *Nature*, 1991, 353, 737-740.

[6] Z. W. Zheng, C. J. Zhao, S. B Lu, Y. Chen, Y. Li, H. Zhang and S. C. Wen, *Opt. Express*, 2012, 20, 23201-23214.

[7] Q. L. Bao, H. Zhang, B. Wang, Z. H. Ni, C. Haley, Y. X. Lim, D. Y. Tang and K. P. Loh, *Nature Photonics*, 2011, 5, 411–415.

[8] H. Tang, G. J. Ehlert and Y. Lin, *Nano Lett.*, 2011, 12, 84-90.

[9] Z. W. Zheng, C. J. Zhao, S. B. Lu, Y. Chen, Y. Li, H. Zhang and S. C. Wen, *Opt. Express*, 2012, 20, 23201-23214.

[10]H. Zhang, S. Virally, Q. L. Bao, K. P. Loh, S. Massar, N. Godbout and P. Kockaert, *Opt. Lett.*, 2012, 37, 1856-1858.

[11]Y. B. Tang, C. S. Lee, J Xu, Z. T. Liu, Z. H. Chen, Z. B. He, Y. L. Cao, G. D. Yuan, H. S. Song, L. M. Chen, L. B. Luo, H. M. Cheng, W. J. Zhang, I. Bello and S. T. Lee, *ACS Nano*, 2010, 4, 3482-3488.

[12]P. N. Zhu, A. S. Nair, S. J. Peng, *ACS Appl. Mater. Interf.*, 2012, 4, 581-585.

[13]Z. M. He, G. H. Guai, J. Liu, C. X. Guo, J. S. C. Loo, C. M. Li and T. T. Y. Tan, *Nanoscale*, 2011, 3, 4613-4616.

[14]O. Frank, M. Bouša and I. Riaz, *Nano Lett.*, 2011, 12, 687-693.

[15]P. E. Hopkins, M. Baraket and E. V. Barnat, *Nano Lett.*, 2012, 12, 590-595.

[16]S. Li, Y. Luo and W. Lv, *Adv. Energy Mater.*, 2011, 1, 486-490.

[17]Z. Zhang, X. Fei, Y. L. Guo, S. Wang and Y. Q. Liu, *ACS Appl. Mater. Interf.*, 2013, 5, 2227-2233.

[18]G. Cheng, M. S. Akhtar, O-B. Yang and F. J. Stadler, *ACS Appl. Mater. Interf.*, 2013, 5, 2227-2233.

[19]J. M. Cai, P. Ruffieux, R. Jaafar, M. Bieri, T. Braun, S. Blankenburg, M. Muoth, A. P. Seitsonen, M. Saleh, X. L.Feng, K. Muellen and R. Fasel, *Nature*, 2010, 466, 470-473.

[20]S. Ito, P. Chen and P. Comte, *Prog. Photovolt.*, 2007, 15, 603-612.

[21]J. Zhang, J. H. Xi and Z. G. Ji, *J. Mater. Chem.*, 2012, 22(34), 17700–17708.

[22]J. Lu, M. Y. Wang, Y. Li and C. H. Deng, *Nanoscale*, 2012, 4, 1577-1580.

[23]J. Zhang, W. Fu, J. H. Xi, H. He, S. C. Zhao, H. W. Lu and Z. G. Ji, *J. Alloys Comp.*, 2013, 575, 40–47.

[24]S. S. Chen, Q. Y. Li, Q. M. Zhang, Y. Qu, H. X. Ji, R. S. Ruoff and W. W. Cai, *Nanotech.*, 2012, 23, 365701.

[25]C. Nethravathi, M. Rajamathi, *Carbon*, 2008, 46, 1994-1998.

[26]J. C. Meyer, A. K. Geim, M. I. Katsnelson, K. S. Novoselov, D. Obergfell, S. Roth, C. Girit and A. Zettl, *Solid State Commun.*, 2007, 143(1-2), 101-109.

[27]Q. J. Xiang, J.G. Yu and M. Jaroniec, *J. Am. Chem. Soc.*, 2012, 134, 6575-6578.

[28] A. Reina, X. Jia, J. Ho, D. Nezich, H. Son and V. Bulovic, *Nano Lett.*, 2009, 9, 30-35.

[29] A. Ismach, C. Druzgalski, S. Penwell, S. Schwartzberg, M. Zheng and A. Javey, *Nano Lett.*, 2010, 10, 1542-1548.

[30] H. Zhang, X. Lv, Y. Li, Y. Wang and J. Li, *ACS Nano*, 2009, 4, 380-386.

[31] Y. L. Liu, W. Shu, K. Q. Chen, Z. Y. Peng and W. Chen, *ACS Catal.*, 2012, 2, 2557-2565.

[32] W. J. Ren, Z. H. Ai, F. L. Jia, X. X. Fan and Z. G. Zou, *Appl. Catal. B: Environ.*, 2007, 69, 138-144.

[33] B. J. Song, H. M. Song and I. T. Choi, *Chem. Eur. J.*, 2011, 17, 11115-11121.

[34] W. Shu, Y. L. Liu, Z. Y. Peng, K. Q. Chen and W. Chen, *J. Alloys Comp.*, 2013, 563, 229-233.

[35] H. Zhang, D. Y. Tang, L. M. Zhao, Q. L. Bao and K. P. Loh, *Appl. Phys. Lett.*, 2010, 96, 111112.

[36] X. Yin, Z. Xue and B. Liu, *J. Power Sources*, 2011,196, 2422-2426.

Figure and Table Captions:

Table 1 Typical performance of DSSCs

Fig. 1 XRD patterns (a) and FTIR spectra (b) of the as-prepared FLG/TiO_2 composites with various graphene contents

Fig. 2 (a) TEM image and (b) HRTEM image of 0.75 wt% FLG/TiO_2 composites (FFT HRTEM image insetted); (c) FFT HRTEM image of the rectangle area in Fig. 2(b)

Fig. 3 (a) Raman map; (b) Raman spectrum (magnified spectrum of 2D band insetted); (c) Raman mapping image of TiO_2 ($E_{g(1)}$ mode) and (d) Raman mapping image of graphene (2D mode) for the 0.75 wt% FLG/TiO_2 composite film

Fig. 4 (a) UV-Vis spectra of the as-prepared FLG/TiO_2 composite films with various graphene contents and (b) the diagram of generating and transferring of the photoexcited electrons in the FLG/TiO_2 composite film

Fig.5 XPS observations of the 0.75 wt% FLG/TiO_2 composites: (a) survey spectrum; (b) C 1s spectrum; (c) Ti 2p spectrum; (d) O 1s spectrum

Fig. 6 (a) Cross-section SEM image of 0.75 wt% FLG/TiO_2 composite film; (b) J-V curves and (c) IPCE measurements of DSSCs of various FLG/TiO_2 composite films

Fig. 7 EIS measurements of DSSCs of various FLG/TiO_2 composite films: (a) Nyquist curves and (b) Bode phase plots

Table 1 Typical performances of DSSCs

wt %	J_{sc} (mA cm^{-2})	V_{oc} (mV)	*FF*	η (%)	R_{ct} (Ω)	C_{μ} (μF)	$\tau = C_{\mu}R_{ct}$ (ms)
0	13.55	651	0.568	5.01	23.1	1275	29.5
0.125	15.22	655	0.587	5.85	22.0	1392	30.6
0.250	16.17	662	0.588	6.29	21.5	1447	31.1
0.500	17.16	672	0.604	6.96	20.7	1585	32.8
0.750	18.03	686	0.667	8.25	18.0	2952	53.1
1.000	17.52	684	0.589	7.06	20.1	2478	49.8

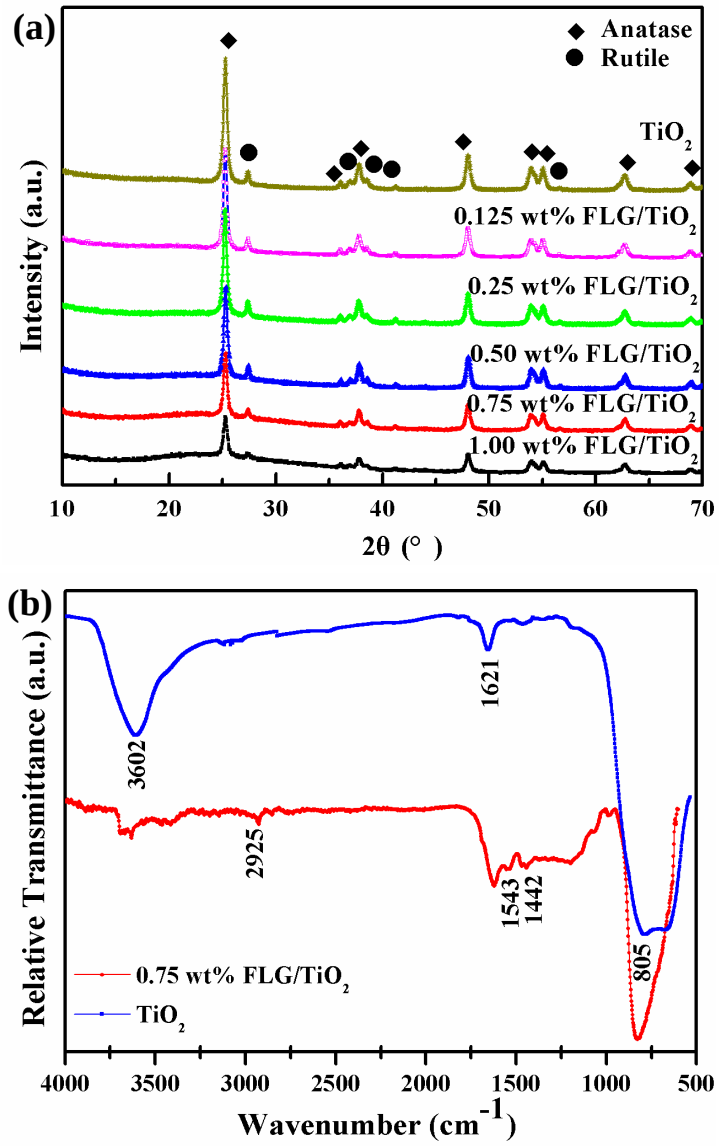

Fig. 1 XRD patterns (a) and FTIR spectra (b) of the as-prepared FLG/TiO_2 composites with various graphene contents

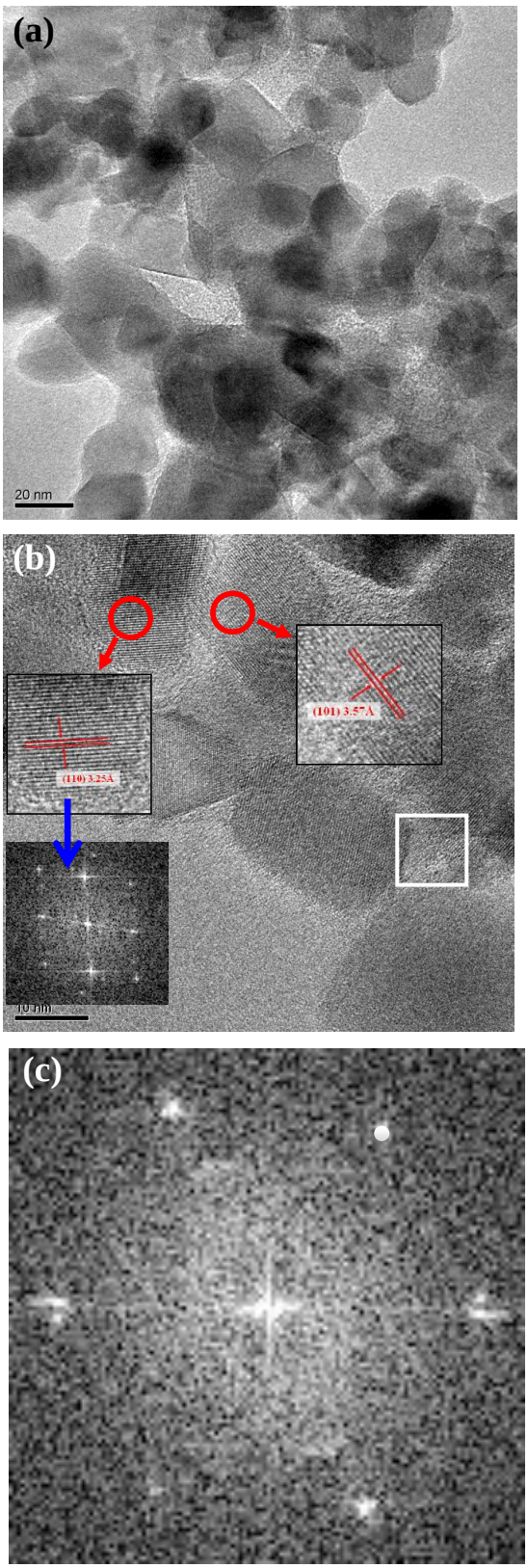

Fig. 2 (a) TEM image and (b) HRTEM image of 0.75 wt% FLG/TiO_2 composites (FFT HRTEM image insetted); (c) FFT HRTEM image of the rectangle area in Fig. 2(b)

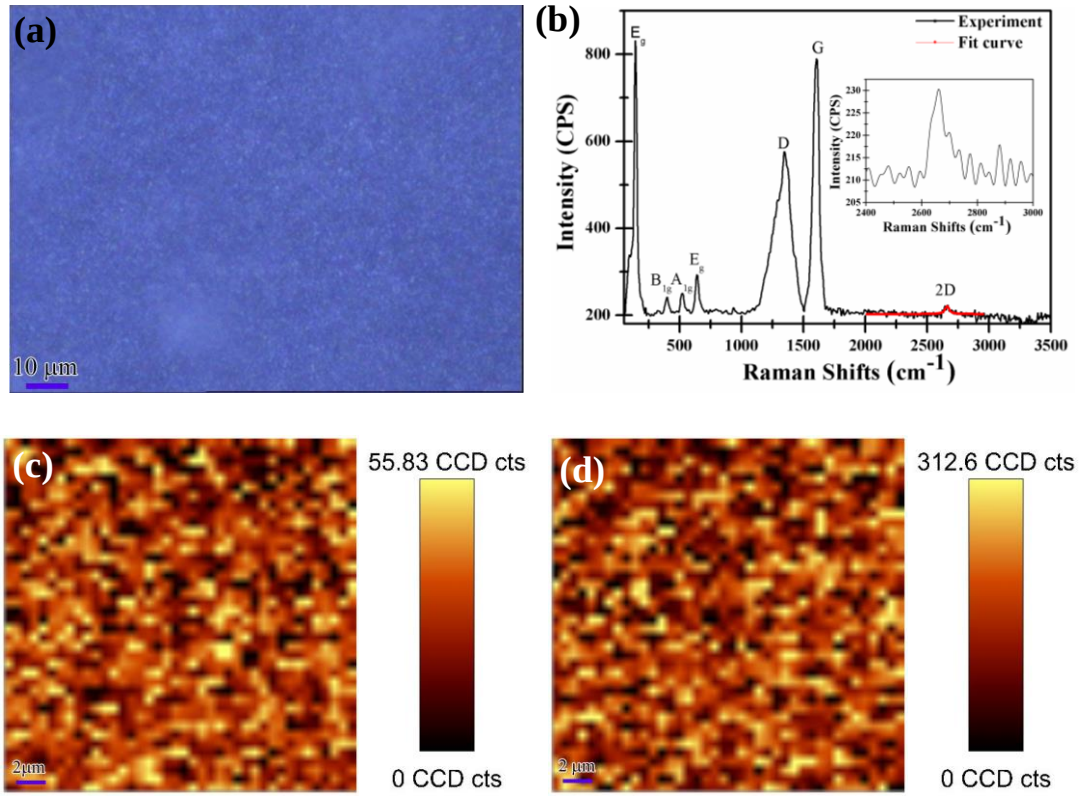

Fig. 3 (a) Raman map; (b) Raman spectrum (magnified spectrum of 2D band insetted); (c) Raman mapping image of TiO_2 ($E_{g(1)}$ mode) and (d) Raman mapping image of graphene (2D mode) for the 0.75 wt% FLG/TiO_2 composite film

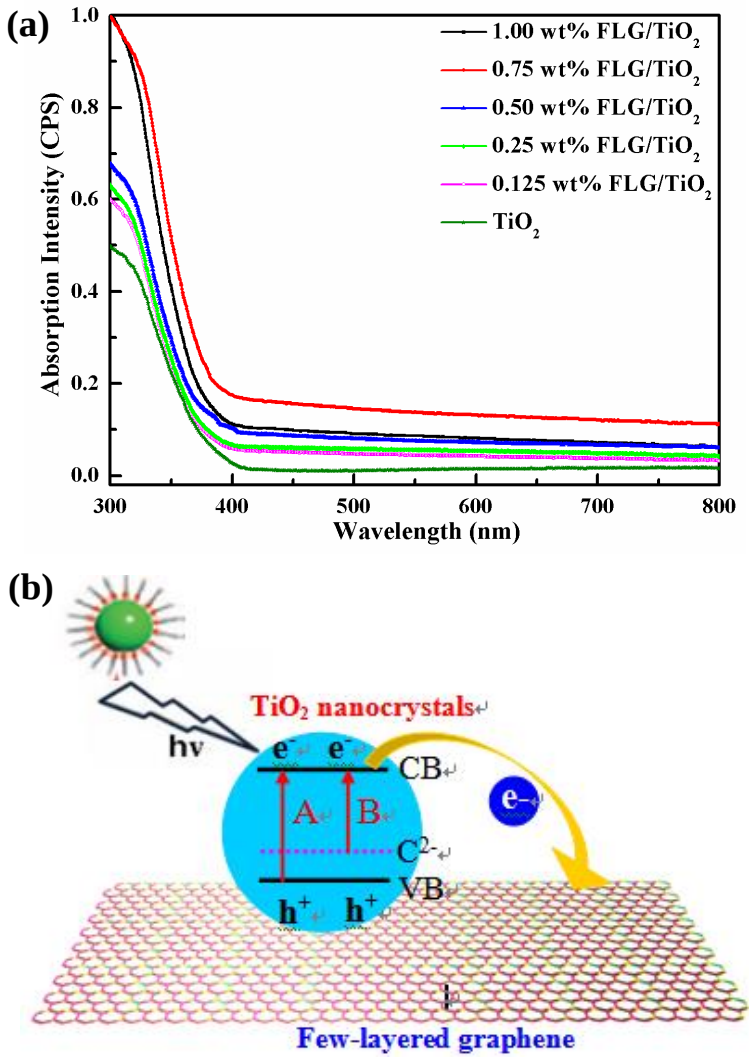

Fig. 4 (a) UV-Vis spectra of the as-prepared FLG/TiO_2 composite films with various graphene contents and (b) the diagram of generating and transferring of the photoexcited electrons in the FLG/TiO_2 composite film

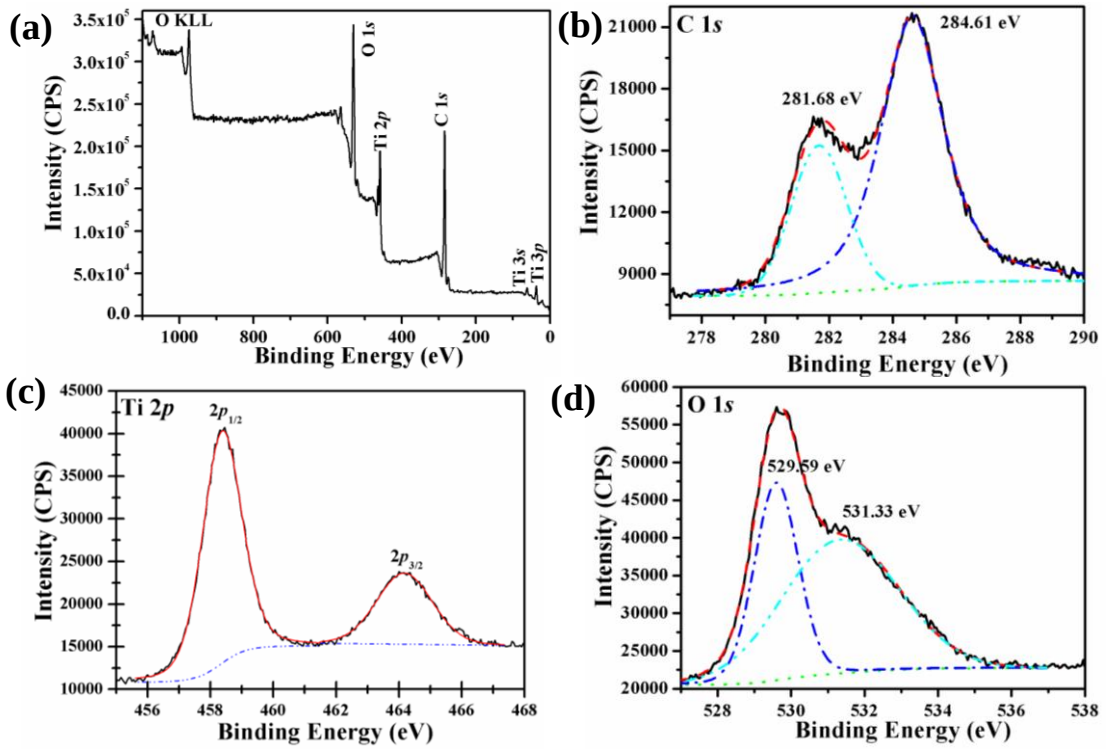

Fig. 5 XPS observations of the 0.75 wt% FLG/TiO_2 composites: (a) survey spectrum; (b) C 1s spectrum; (c) Ti 2p spectrum; (d) O 1s spectrum

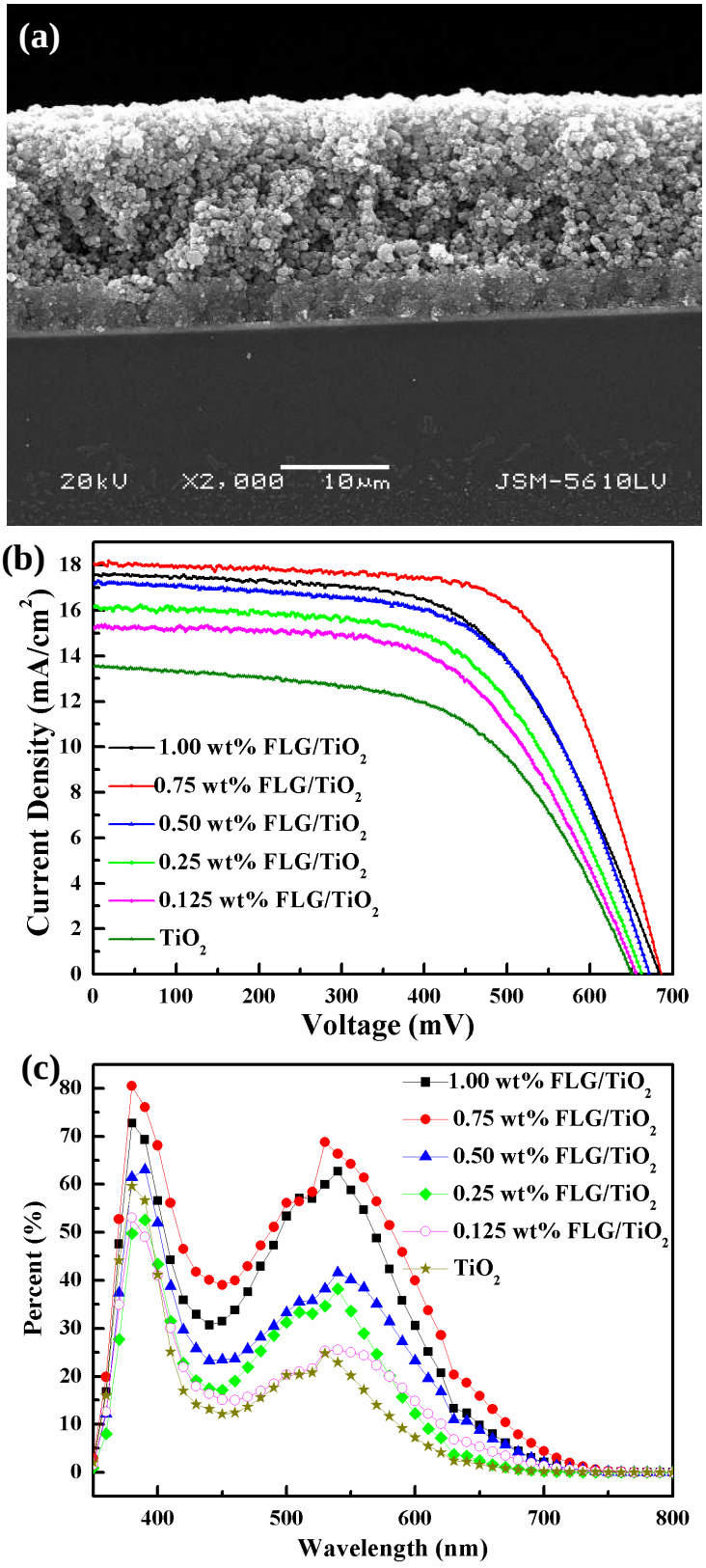

Fig. 6 (a) Cross-section SEM image of 0.75 wt% FLG/TiO_2 composite film; (b) J-V curves and (c) IPCE measurements of DSSCs of various FLG/TiO_2 composite films

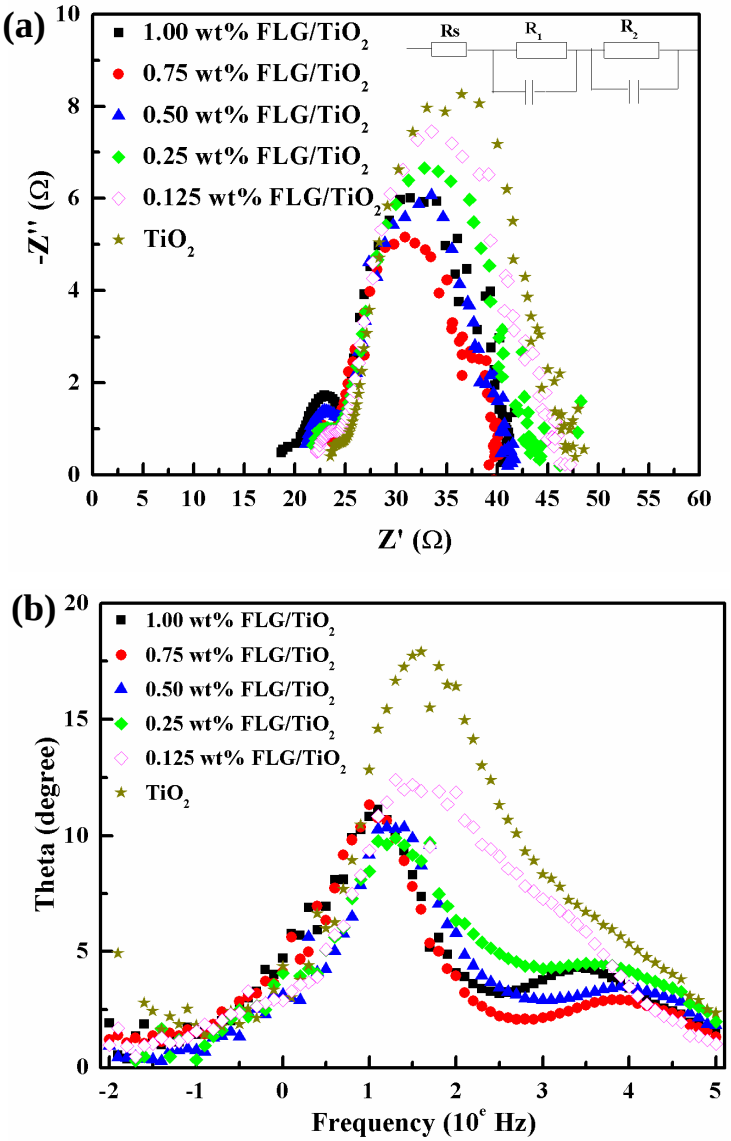

Fig. 7 EIS measurements of DSSCs of various FLG/TiO_2 composite films: (a) Nyquist curves and (b) Bode phase plots